NASA TECHNICAL NOTE

NASA TN D-7722

NASA TN D-7722

BARIUM CLOUD EVOLUTION AND STRIATION FORMATION IN THE MAGNETOSPHERIC RELEASE ON SEPTEMBER 21, 1971

by David Adamson and Clifford L. Fricke

Langley Research Center
Hampton, Va. 23665

NATIONAL AERONAUTICS AND SPACE ADMINISTRATION • WASHINGTON, D. C. • SEPTEMBER 1974

1. Report No. NASA TN D-7722	2. Government Accession No.	3. Recipient's Catalog No.
4. Title and Subtitle BARIUM CLOUD EVOLUTION AND STRIATION FORMATION IN THE MAGNETOSPHERIC RELEASE ON SEPTEMBER 21, 1971		5. Report Date September 1974
		6. Performing Organization Code
7. Author(s) David Adamson and Clifford L. Fricke		8. Performing Organization Report No. L-9668
9. Performing Organization Name and Address NASA Langley Research Center Hampton, Va. 23665		10. Work Unit No. 879-11-36-01
		11. Contract or Grant No.
12. Sponsoring Agency Name and Address National Aeronautics and Space Administration Washington, D.C. 20546		13. Type of Report and Period Covered Technical Note
		14. Sponsoring Agency Code

15. Supplementary Notes

16. Abstract

    The joint NASA-Max Planck Institute Barium Ion Cloud (BIC) Experiment on September 21, 1971, involved the release of 1.7 kg of neutral barium at an altitude of 31 500 km at a latitude of 6.93° N. and a longitude of 74.40° W. A theoretical model describing the barium neutral cloud expansion and the ion cloud formation is developed. The mechanism of formation of the striational features observed in the release is also discussed. Two candidate instabilities, which may contribute to striation formation, are examined. The drift instability stemming from the outwardly directed drag force exerted on the ions by the outstreaming neutrals is rejected on the grounds that the ion density is too low during the collision-dominated phase of the cloud expansion to support this kind of instability. The joint action of Rayleigh-Taylor and flute instabilities plausibly accounts for the observed striational structure. This same mechanism may well be operative at times of sudden injection of plasma into the inner magnetosphere during geomagnetic storms and may thus contribute to the formation of field-alined inhomogeneities which serve as whistler ducts.

17. Key Words (Suggested by Author(s)) Plasma instabilities Magnetospheric physics Barium ion clouds	18. Distribution Statement Unclassified — Unlimited STAR Category 13

19. Security Classif. (of this report) Unclassified	20. Security Classif. (of this page) Unclassified	21. No. of Pages 43	22. Price* $3.25

*For sale by the National Technical Information Service, Springfield, Virginia 22151

BARIUM CLOUD EVOLUTION AND STRIATION FORMATION IN THE
# MAGNETOSPHERIC RELEASE ON SEPTEMBER 21, 1971

By David Adamson and Clifford L. Fricke
Langley Research Center

SUMMARY

The joint NASA-Max Planck Institute Barium Ion Cloud (BIC) Experiment on September 21, 1971, involved the release of 1.7 kg of neutral barium at an altitude of 31 500 km at a latitude of 6.93^O N. and a longitude of 74.40^O W. A theoretical model describing the barium neutral cloud expansion and the ion cloud formation is developed. The mechanism of formation of the striational features observed in the release is also discussed. Two candidate instabilities, which may contribute to striation formation, are examined. The drift instability stemming from the outwardly directed drag force exerted on the ions by the outstreaming neutrals is rejected on the grounds that the ion density is too low during the collision-dominated phase of the cloud expansion to support this kind of instability. The joint action of Rayleigh-Taylor and flute instabilities plausibly accounts for the observed striational structure. This same mechanism may well be operative at times of sudden injection of plasma into the inner magnetosphere during geomagnetic storms and may thus contribute to the formation of field-alined inhomogeneities which serve as whistler ducts.

INTRODUCTION

In the presence of a magnetic field plasmas tend to form field-alined inhomogeneities or striations. This tendency manifests itself in a variety of ways throughout nature. Perhaps the most spectacular example is provided by the striated or rayed aurora. Another instance is the existence in Earth's magnetosphere of field-alined tubes of enhanced electron density which serve as guides to the whistler mode of wave propagation. On a larger scale, visual evidence is noted in the filamentary structures of the solar corona and in the prominences which occur within it (fig. 1). On an even grander scale, the filamentary structures in gaseous nebulae may plausibly be argued to be manifestations of the same phenomena. The fact that in all of these phenomena the striations are field-alined does not imply a common underlying mechanism of formation. It is simply a consequence of the fact that in tenuous plasmas the conductivity along the magnetic field lines is substanially greater than the conductivity transverse thereto, and the same electrodynamic forces are therefore operative at all points along the same magnetic field line.
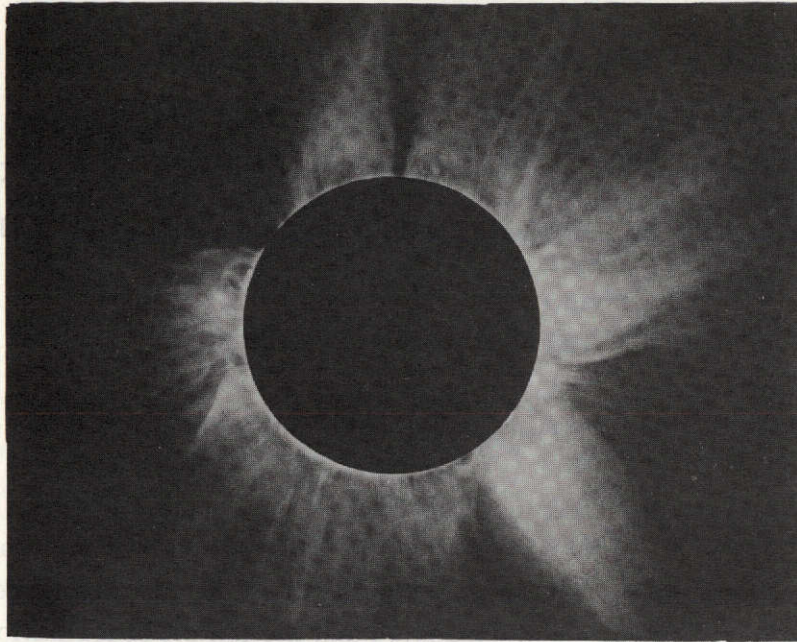
L-74-1138

Figure 1.- Filamentary structure of solar corona.
Photograph of solar eclipse on March 7, 1970,
taken and processed by Leonard M. Weinstein
of NASA LRC and Sheldon M. Smith of NASA
ARC.

In view of the widespread occurrence of filamentary structures in naturally occur-
ring plasmas, it is hardly surprising that striations are invariably observed in barium
ion cloud releases in the ionosphere. In certain of the releases at high latitude (ref. 1)
there are strong indications that some of the striational features result from the barium
ions acting as tracers in delineating magnetic field inhomogeneities preexisting the
release. In other cases the regularity of the striational features coupled with their pro-
pensity to form in the proximity of the trailing edge of the cloud leads to the speculation
that their formation stems from some inherent instability triggered by interaction with
the ambient medium. A number of theoretical investigations into the nature of the insta-
bilities contributing to striation formation in barium clouds released at ionospheric lati-
tudes have recently been made (refs. 2 to 6). The theories advanced for the explanation
of these instabilities in ion clouds in the ionosphere all emphasize the importance of the
role played by collisions between the drifting ions and the neutral component of the ambient
medium.

Two experiments involving barium releases deep within the magnetosphere have been
made. In the first experiment (ref. 7) about 100 grams of barium were released at an

2

altitude of about 11.5 Earth radii (about 75 000 km) from the European Space Research Organization (ESRO) Highly Eccentric Orbiting Satellite (HEOS I) on March 18, 1969. One or two faint striational features were observed. The appearance of these striations in the almost perfect vacuum existing at such a long distance from Earth was attributed to flute instabilities operative during the initial phase of cloud expansion (ref. 8). The second experiment made on September 21, 1971, on which this paper is based, involved the release of 1.7 kg of barium at an altitude of 31 500 km (ref. 9). Considerable striational structure, consisting of about a dozen prominent striational features, evolved within the first 2 minutes and remained visible for about 30 minutes. Since the purpose of this paper is to investigate the nature of the instabilities which contribute to striation formation, consideration is limited to the early phase of cloud expansion.

In the section entitled "Observational Data" a brief description is given of the observational data bearing on striation formation and structure. In the section entitled "Cloud Model" a theoretical model, which purports to describe the early time evolution of the barium neutral cloud and the formation of the ion cloud, is developed. Subsequent sections are devoted to a discussion of drift instability and Rayleigh-Taylor and flute instabilities and the role they may play in striation formation.

SYMBOLS

a_e classical radius of electron

$\vec{b}$ unit vector in direction of magnetic field

$\vec{B}$ magnetic-field vector

B_e strength of magnetic field outside ion cloud

c velocity of light

C constant appearing in expression for rate of ionization of neutral cloud

d offset distance of line of sight from cloud center

e electron charge

$\vec{E}$ electric field vector

f oscillator strength

F	flux of radiant energy
g	acceleration of cloud boundary, $\dfrac{d^2 r_m}{dt^2}$
G(v,t)	function defined in equation (14)
I_0	differential flux of radiant energy (flux per unit frequency range)
$\vec{j}$	electric current vector
k	wave number of boundary perturbation; Boltzmann constant
k'	absorption coefficient per unit volume
K	constant
l	length of cloud profile arc
L	length of ion cloud measured along cloud axis
m	electron mass
n	number density of neutral atoms
n_i	number density of ions
N(t)	total number of neutral barium atoms as a function of t
$\Delta N(t)$	number of neutral atoms having radial velocities in range v to $v + \Delta v$ at time t
$N_i(t)$	total number of barium ions as a function of t
p	plasma pressure
q	mode of fluting of boundary perturbation
r	radial distance from neutral cloud center; distance from ion cloud axis

r_m	equatorial radius of unperturbed ion cloud boundary
R	radius of curvature of magnetic field line
$\vec{R}$	radius of curvature vector
s	distance measured along boundary in direction of magnetic field
t	time elapsed from instant of cloud release
u	velocity component of neutral barium atoms in direction of solar irradiation
v	radial velocity of neutral atoms
v_o	mean radial velocity of neutral atoms
v_T	radial velocity spread of neutral atoms
v_{th}	average thermal velocity of ions
x	axis pointing toward source of irradiation
z	distance along cloud axis
α	exponential growth of instabilities (absence of thermal quenching)
$\overline{\alpha}$	exponential growth of instabilities (presence of thermal quenching)
$\beta = \dfrac{g}{r_m} + \dfrac{5}{8}\dfrac{B_e^2}{\rho L^2}$	
γ	frequency width of spectral line
ϵ	ratio, $\dfrac{\text{Radius increment from undeformed profile to crest}}{\text{Radius of undeformed profile}}$
η	radial distance from unperturbed cloud boundary (positive outwards)
$\delta\eta$	amplitude of boundary perturbation

κ constant appearing in exponential damping factor associated with thermal damping of instability

λ wavelength of spectral line

λ_c circumferential wavelength of boundary perturbation of ion cloud

$\mu = CI_0\gamma$

μ_0 magnetic permeability

ν frequency of spectral line

$\xi = \dfrac{v_0}{v_T}$

ρ plasma density

σ variable of integration

τ variable of integration

τ_d time for ion to move between crests and troughs of fluted ion cloud boundary

ϕ azimuthal angle

Φ brightness parameter $\left(\text{particles per cm}^2 \text{ column along line of sight}\right)$

Subscripts:

o values at unperturbed boundary of ion cloud

e values at instant of pressure equalization

max maximum

In the stability analysis, tilde over a quantity denotes its unperturbed value.

OBSERVATIONAL DATA

On September 21, 1971, 1.7 kg of barium were released at an altitude of about 31 500 km, a latitude of 6.93° N. and a longitude of 74.40° W. The barium was produced by a thermite-type chemical reaction and vented into space as a neutral cloud. Under solar irradiation the neutral barium was almost completely ionized within the first minute. The ions, as they formed, spiraled upwards and downwards along Earth's magnetic field lines, the ion cloud as a whole elongating therefore along the magnetic field direction. Figure 2(a) is a photograph of the release taken 2 minutes 27 seconds after release with a Baker-Nunn camera located at Mount Hopkins, Arizona. The spherical neutral cloud consists of strontium, which was present in the payload as an impurity (the barium having been completely ionized at this epoch). Note that the neutral cloud exhibits the shell-like structure invariably accompanying the explosive expansion of neutral clouds in the hard vacuum of space existing at altitudes in excess of 500 km (ref. 10). The bar through the center of the neutral cloud comprises the main core of the barium ion cloud. The fact that at early times the ion cloud remains centered on the neutral cloud, which moves with the velocity of the rocket, results from the buildup of polarization charges within the ion cloud interior (ref. 11). Another feature in this photograph worthy of note is the existence of striational features on both sides of the main core. The fuzzy appearance of the striations at these early times is attributed in part from limitations of resolution of the camera system used and in part from obscuration of the thin filaments by the neutral cloud in which they are engulfed. The photograph in figure 2(b) was taken 19 minutes 8 seconds after release with a 70-mm f/1 image intensified optical system located at Cerro Morado, Chile. At this time considerable striational structure is discernible. The regularity of the spacing of those striations contiguous to the main core precludes their being interpreted as delineations of naturally occurring inhomogeneities in the magnetic field preexisting the release.

In figure 3 the angular separations from the main core of all identifiable striational features are presented as functions of time for the period 16 minutes following release. This figure incorporates data obtained by using an image intensified optical system located at White Sands, New Mexico. For each photographic frame the coordinates of one point on each of the discernible striational features were read on a Telereader and automatically recorded on punched cards. The angular distances between the main core and the striations were computed by using two known stars as a reference and plotted as in figure 3 with a computer plotting system. The main core lies along the abscissa axis and at any epoch a section perpendicular to this axis defines the apparent angular displacement in degrees of the striational features relative to the main core, as viewed from White Sands, New Mexico. Although no reliable data exist on striation separation during the first 4 minutes as a result of obscuration of the striational features by the overlying neutral
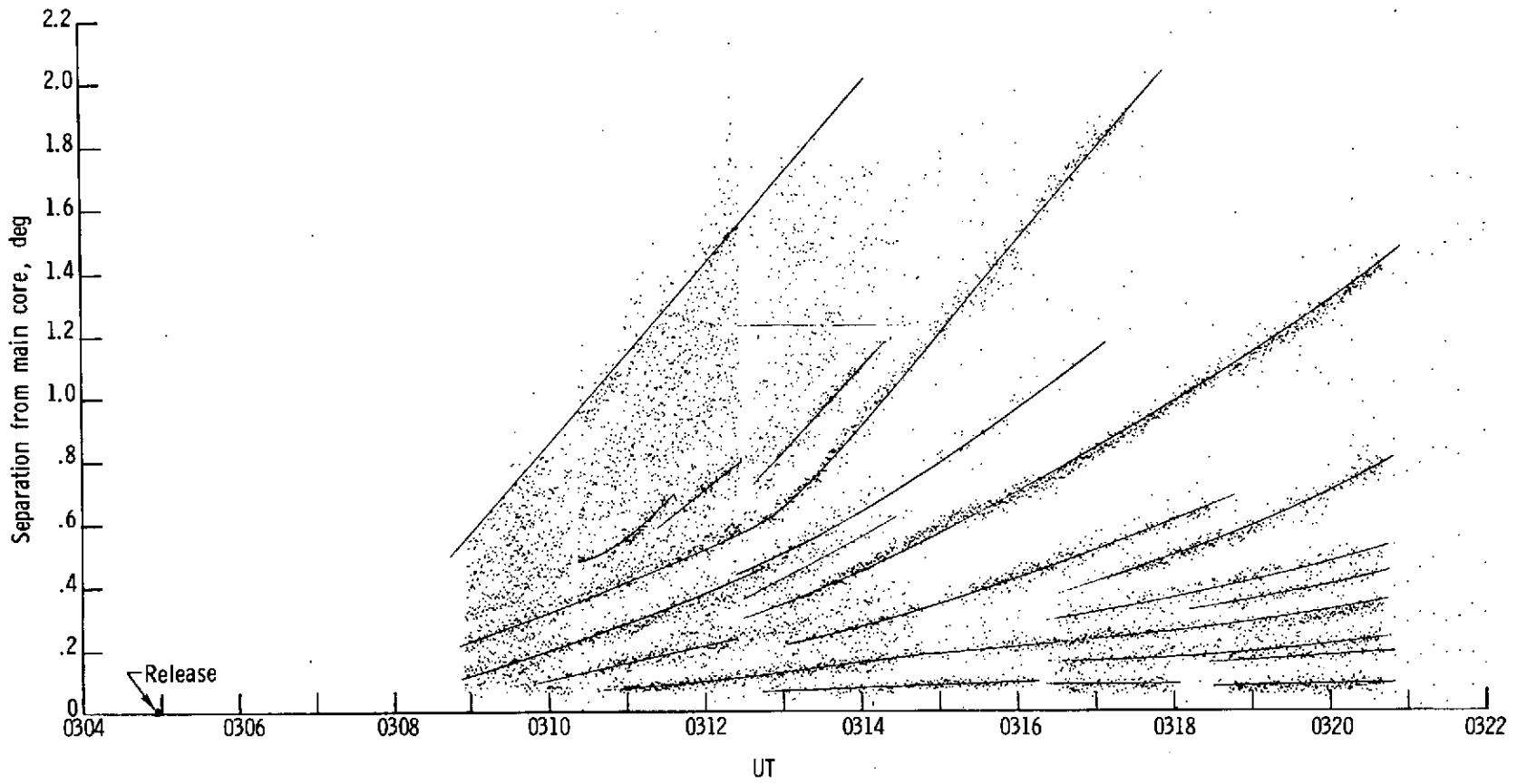
(a) Photograph taken at Mount Hopkins, Arizona (2 min 27 sec after release).
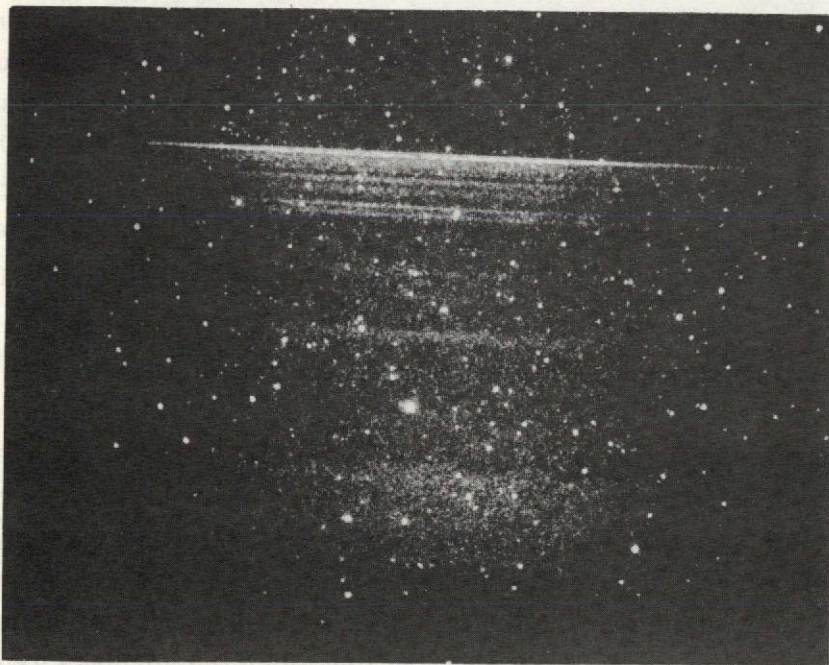
L-74-1139

(b) Photograph taken at Cerro Morado, Chile (19 min 8 sec after release).

Figure 2.- Photographs of barium cloud and component striations.

8

Figure 3.- Angular separation from main core (as viewed from White Sands, New Mexico) of identifiable striational features as function of time.

cloud (though a 200 Å interference filter was used, the closeness of the spectral lines of ionized barium, 4554 Å, and neutral strontium, 4607 Å, precluded their separation), the tendency of the striations to converge on the release point can be noted, thereby indicating that the striations did form, through some intrinsic instability, during the transient phase of cloud expansion. This conclusion is further reinforced by data obtained with a highly sensitive image-intensified television camera system (ref. 12).

CLOUD MODEL

The purpose of the present section is to derive expressions for the density distributions of particles comprising both the neutral and the ionized barium clouds as functions of position and time. Such data are needed as input to the subsequent stability considerations.

The following assumptions underlying the present analysis are listed together with some pertinent comments pertaining thereto:

(1) The barium atoms comprising the neutral cloud are released simultaneously and move radially outward without collisions. From a prior experiment (ref. 13) the mean velocity of radial expansion v_o is known to be approximately equal to 1200 m/sec and the thermal velocity spread v_T about the mean is approximately equal to 150 m/sec. (As a result of the mean velocity being so much larger than the velocity spread, the neutral cloud exhibits the shell-like structure so evident in fig. 2(a).) By virtue of the almost explosive expansion of the barium neutral cloud into the hard vacuum of space, the collisions cease to play a role after the first second or two and can therefore be ignored.

(2) The ionization process is dominantly controlled by absorption at a single wavelength. The ionization process is in fact a complex one involving a number of transitional steps (ref. 14). As in all such chain reactions the slowest one controls the rate of ionization. Therefore, for the purposes of the present calculation, ionization may be regarded as a single-step process resulting from absorption at the wavelength of the pacing transition.

(3) The spectral line associated with the pacing transition is rectangular in form and has a frequency width γ in hertz.

(4) The ions, once formed, spiral along the magnetic field lines with a velocity component along the field line equal to that of the parent neutral atom. During ionization an excess of energy is imparted to the electrons, and this is subsequently shared with the ions; however, as a consequence of the large mass disparity, the effect on the ions is small. In the barium release on September 21, 1971, the rate of cloud elongation built up slowly to an unexpectedly high value over a period of several minutes (ref. 9). However, since the transient phase of cloud expansion, which is solely of interest in the present analysis, lasted less than a minute, this slow energization of the ions need not be considered.

(5) The ion gyroradius is small when compared with the cloud diameter. If the radially outward velocity of the ions as they are formed is assumed to be the same as that of the parent atom, that is, approximately 1 km/sec, the ion gyroradius corresponding to a magnetic field strength of 150 gammas existing at the altitude of release is about 60 km. This is much larger than the observed cloud radius of about 8 km at later times, and on these grounds the validity of this assumption may, therefore, be questioned. However, bear in mind that the effect of the electrons, which will remain tied tightly to the magnetic field lines, will be to inhibit the orbital motions of the ions, thus materially reducing the effective ion gyroradius. This is borne out by the numerical studies of initial cloud expansion described in reference 15.

(6) The magnetic field lines remain undistorted during ion cloud formation. At very early times, prior to striation formation, the magnetic field lines are probably excluded from the cloud interior. This is borne out by the numerical studies reported in reference 15 in which the condition of radial symmetry is enforced. During the striation growth and detachment the field lines would be expected to infiltrate the cloud interior. So little is known about this infiltration process that it cannot be adequately incorporated into a cloud model. Thus in formulating a cloud model, the following two alternatives exist: (a) To assume complete exclusion of magnetic field lines, in which case the model would be more realistic at very early times; or (b) to assume the field lines to permeate the cloud interior, in which case the model would be more realistic at later times. In the present formulation the latter course has been chosen.

Evolution of Neutral Cloud

In figure 4 the spherical neutral cloud is depicted as being irradiated with sunlight from the right. Since the atoms are assumed to be released instantaneously and move without collisions, those occupying the disk AA will all have velocity components in the x-direction in the range u to $u + \Delta u$. The disk thus advances to the right with velocity u, distending in the radial direction as it does so. The thickness of the disk at any instant is given by the expression $\Delta x = t \Delta u$ where t is the time elapsed from the instant of release. Clearly, the velocity gradient in the x-direction is uniform across the entire cloud and given by

$$\frac{\Delta u}{\Delta x} = \frac{1}{t} \tag{1}$$

Since the Doppler shift of the absorption band, and hence the ionization, is wholly independent of the velocity component perpendicular to x (x points toward the irradiating source), the problem can be conceptually simplified by treating it as a two-dimensional slab dilating in the x-direction, as represented in figure 5. Without loss of generality, the arbitrary section XX is assumed to be at rest. The crosshatched swath superimposed in
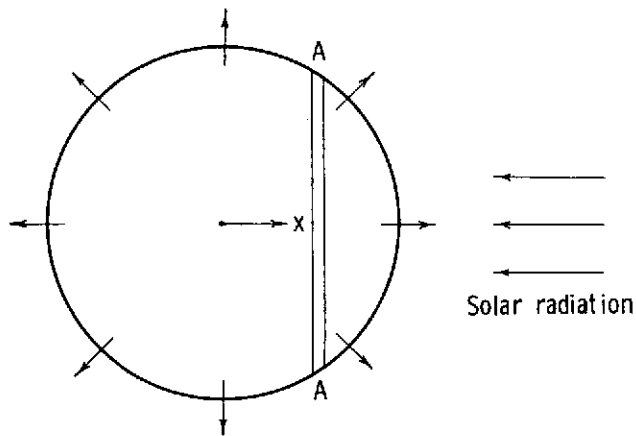
Figure 4.- Expanding neutral cloud.

figure 5 serves to define, on the frequency scale on the left, the absorptive frequency range as a function of cross-section location. Thus, at section XX the range of absorbed frequencies extends from ν_a to ν_b. A section to the right of XX will be moving to the right and its absorptive waveband will therefore be Doppler shifted to lower frequencies and vice versa.
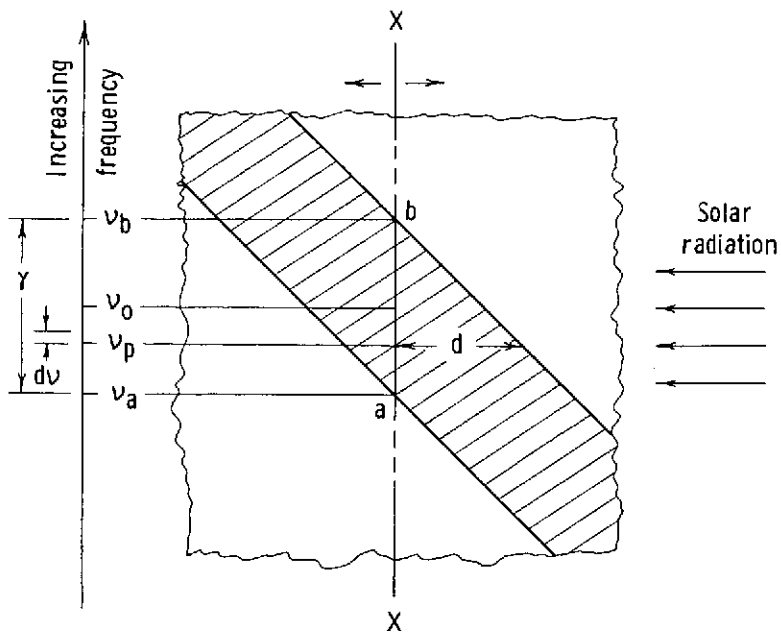

Figure 5.- Dilating slab.

The Doppler shift as a function of velocity is given by

$$\frac{\Delta\nu}{\Delta u} = \frac{1}{\lambda} \tag{2}$$

From equations (1) and (2), where λ is the wavelength, the expression for the slope of the absorptive waveband in figure 5 is

$$\frac{\Delta\nu}{\Delta x} = \frac{1}{\lambda t} \tag{3}$$

The radiation, in the frequency range $d\nu$ centered on ν_p, incident on the plane XX is subjected to prior absorption only within the slab of thickness d (fig. 5). By setting $\sigma = \frac{\nu_p - \nu_o}{\gamma}$ and using equation (3)

$$d = \left(\frac{1}{2} + \sigma\right)\gamma\lambda t \tag{4}$$

Denoting the unattenuated differential flux (flux per unit frequency range) of radiation, assumed constant over the width of the spectral line, by I_o, the radiation incident on the plane XX in the frequency range $d\nu$ is given by

$$dF = I_o e^{-k'd} \, d\nu \tag{5}$$

where k' is the absorption coefficient per unit volume.

By assumption (3), k' is constant over the entire bandwidth γ and equal to (see ref. 16)

$$k' = \frac{2nfe^2}{mc\gamma} \tag{6}$$

where

n   number density

f   oscillator strength

e   electron charge

m   mass of the electron

c   velocity of light

γ spectral line width

By substituting equations (4) and (6) in equation (5) and integrating over the entire line width, the expression for the integrated flux at section XX is

$$\text{Integrated flux} = I_o \int_{-1/2}^{+1/2} \exp\left[-\frac{2nfe^2\lambda t}{mc}\left(\frac{1}{2} + \sigma\right)\right]\gamma \, d\sigma$$

$$= \frac{I_o\gamma mc}{2nfe^2\lambda t}\left[1 - \exp\left(-\frac{2nfe^2\lambda t}{mc}\right)\right] \tag{7}$$

A comment is called for at this point regarding the derivation of equation (7). Note that implicit in equation (5) is the assumption that the density is uniform throughout the absorptive layer, whereas in the actual case of the barium cloud density gradients do exist. Furthermore, the outermost layers of the expanding spherical cloud are not screened by overlying layers as is assumed in the foregoing analysis. For equation (7) to be applicable to the neutral barium cloud, the thickness of the absorbing layer must be small compared with the thickness $v_T t$ of the spherical shell of the cloud within which the bulk of the barium resides.

The total thickness of the absorbing layer contributing to flux attenuation at a given section, as obtained from equation (4) by setting $\sigma = \frac{1}{2}$, is equal to $\gamma\lambda t$. Thus the ratio of thickness of absorptive layer to shell thickness is given by $\gamma\lambda/v_T$.

By substituting the expression $\frac{4\pi\nu^2 e^2}{3mc^3}$ (see ref. 16) for spectral line width γ and making use of the fact that the classical radius of the electron a_e is equal to $\frac{e^2}{mc^2}$

$$\frac{\text{Thickness of absorptive layer}}{\text{Shell thickness}} = \frac{4\pi c a_e}{3\lambda v_T} \tag{8}$$

By assuming a v_T of 150 m/sec and a λ of 5000 Å, this ratio is found to be less than 0.05, which is small enough to justify using equation (7) throughout the following analysis.

The rate at which neutral atoms are being ionized, and hence lost to the neutral population, is proportional to the radiation flux and the neutral particle density n. Thus

$$\frac{dn}{dt} = -CFn \tag{9}$$

By substituting equation (7)

$$\frac{dn}{dt} = -\frac{\mu mc}{2fe^2\lambda t}\left[1 - \exp\left(\frac{-2nfe^2\lambda t}{mc}\right)\right] \tag{10}$$

14

where

$$\mu = CI_o\gamma$$

Denote by ΔN the number of neutral atoms having radial velocities in the range v to $v + \Delta v$. At the instant t these atoms occupy a spherical shell having an inner radius tv and a thickness $t\,\Delta v$. Hence from equation (10) the instantaneous rate of ionization per unit volume is given at all points within the spherical shell by the expression

$$\frac{-\mu mc}{2fe^2\lambda t}\left[1 - \exp\left(\frac{-fe^2\lambda\,\Delta N}{2\pi mct^2v^2\Delta v}\right)\right]$$

from whence it follows that by multiplying by the volume of the shell

$$\frac{d(\Delta N)}{dt} = \frac{-\mu mc}{2fe^2\lambda t}\left[1 - \exp\left(\frac{-fe^2\lambda\,\Delta N}{2\pi mct^2v^2\Delta v}\right)\right]4\pi t^3v^2\Delta v$$

$$= -\mu t^2\frac{2\pi mcv^2\Delta v}{fe^2\lambda}\left[1 - \exp\left(\frac{-fe^2\lambda\,\Delta N}{2\pi mct^2v^2\Delta v}\right)\right] \tag{11}$$

From an analysis of neutral cloud expansion in other high-altitude neutral barium cloud releases (ref. 13), the initial velocity distribution has been found to be of the form

$$\Delta N = K\left\{\exp\left[-\left(\frac{v - v_o}{v_T}\right)^2\right]\right\}v^2\Delta v \tag{12}$$

Thus, the initial total number of neutral atoms $N(0)$ is given by

$$N(0) = K\int_0^\infty\left\{\exp\left[-\left(\frac{v - v_o}{v_T}\right)^2\right]\right\}v^2dv$$

$$= Kv_T^3\left\{\frac{\pi^{1/2}}{2}\left(\xi^2 + \frac{1}{2}\right)\left[1 + P(\xi)\right] + \frac{\xi}{2}e^{-\xi^2}\right\}$$

where

$$\xi = \frac{v_o}{v_T}$$

and

$$P(\xi) = \frac{2}{\pi^{1/2}}\int_0^\xi e^{-x^2}dx$$

Since ξ is approximately equal to 8, then to a sufficient accuracy

$$K = \frac{N(0)}{\pi^{1/2}\left(\xi^2 + \frac{1}{2}\right)v_T^3}$$

By introducing the constant into equation (12), it follows that at $t = 0$, the total number of neutral atoms in the range v to $v + \Delta v$ is given by

$$\Delta N(0) = \frac{N(0)}{\pi^{1/2}\left(\xi^2 + \frac{1}{2}\right)v_T^3} \exp\left[-\left(\frac{v - v_o}{v_T}\right)^2\right] v^2 \Delta v \tag{13}$$

The function

$$G(v,t) = \frac{fe^2\lambda \, \Delta N(t)}{2\pi mcv^2 \Delta v} \tag{14}$$

is introduced and substituted into equations (11) and (13). Thus

$$\frac{dG(v)}{dt} = -\mu t^2\left[1 - \exp\left(-\frac{G}{t^2}\right)\right] \tag{15}$$

and

$$G(v,0) = \frac{fe^2\lambda N(0)}{2\pi^{3/2}mc\left(\xi^2 + \frac{1}{2}\right)v_T^3} \exp\left[-\left(\frac{v - v_o}{v_T}\right)^2\right] \tag{16}$$

Equations (15) and (16) determine $G(v,t)$. The total number of neutral atoms is obtained by summing over all subsets

$$N(t) = \sum \Delta N(t) = \sum \frac{2\pi mcv^2 \Delta v}{fe^2\lambda} G(v,t)$$

In the integral limit

$$N(t) = \frac{2\pi mc}{fe^2\lambda} \int_0^\infty G(v,t)v^2 dv \tag{17}$$

The total number of barium ions

$$N_i(t) = N(0) - \frac{2\pi mc}{fe^2\lambda} \int_0^\infty G(v,t)v^2 dv \tag{18}$$

As mentioned earlier from an analysis of the data obtained on a previous high-altitude release (ref. 13), the mean radial velocity of the neutral barium atoms v_o and their velocity spread v_T have been found to be approximately equal to 1200 m/sec and 150 m/sec, respectively. In addition, the amount of barium released on September 21, 1971, has been estimated at 1.7 kg $\left(N(0) = 7.45 \times 10^{24}\right)$. This estimate is based on an analysis of photometric data (ref. 17). The parameter μ appearing in equation (15) has been determined from earlier investigations (ref. 13) to be equal to 0.05. The remaining parameter $f\lambda$ depends on the nature of the pacing transition involved in the ionization process, which remains unidentified, and must be regarded as an unknown. By varying this parameter and matching the predicted time dependence of the total number of ions as calculated from equation (18) against the observed time dependence as deduced in reference 17 from the photometric variation of ionized cloud brightness at 4554 Å, it was found that the best fit over the initial 50 seconds was obtained by assigning $f\lambda = 1500$ Å. The excellent agreement obtained is clearly exhibited in figure 6.
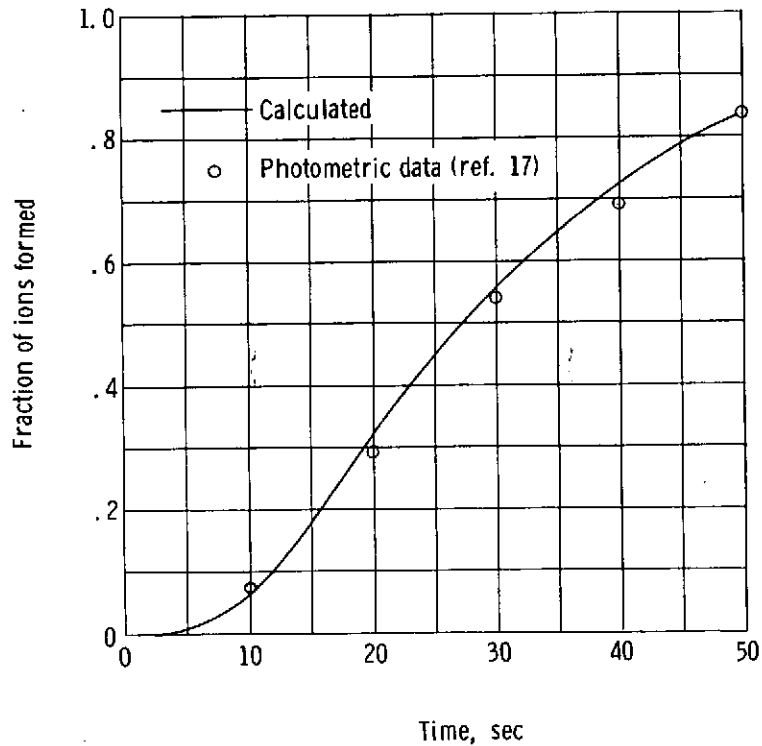

Figure 6.- Fraction of ions formed as function of time.

At epoch t the neutral atoms populating the spherical shell of inner radius r and thickness Δr have velocities in the range $v = \frac{r}{t}$ and $\Delta v = \frac{\Delta r}{t}$.

Hence, from equation (14) the number of neutral atoms between r and $r + \Delta r$ at epoch t is equal to

$$\frac{2\pi mc \left(\frac{r}{t}\right)^2 \frac{\Delta r}{t}}{fe^2 \lambda} G\left(\frac{r}{t},t\right)$$

Thus the density of neutral atoms at r,t is given by

$$n(r,t) = \frac{mc}{2fe^2 \lambda t^3} G\left(\frac{r}{t},t\right) \tag{19}$$

The neutral density obtained from this equation is plotted against r for the four epochs, 10, 20, 30, and 40 seconds in figure 7. Note that the density peak propagates outwards at a rate equal to the mean radial velocity of the neutral atoms of 1200 m/sec. Note also that the vertical scales are different at the four epochs. This difference was necessitated by the rapid falloff of neutral density resulting in part from the cloud expansion and in part from the rapid ionization.

Variation of Density Within Ion Cloud

For simplicity only the ion distribution in the median plane, drawn through the cloud center perpendicular to the field lines, will be considered. The density of neutral atoms at instant τ in the proximity of the point P a distance r from the origin (fig. 8) is given by equation (19). By noting that the rate of formation of ions is equal to the rate of decrease of the neutral population, the following expression for the number of ions deposited within unit volume centered on P in the interval $d\tau$ is obtained from equations (19) and (10)

$$dn_i = \frac{\mu mc}{2fe^2 \lambda \tau} \left\{ 1 - \exp\left[-\frac{1}{\tau^2} G\left(\frac{r}{\tau},\tau\right) \right] \right\} d\tau \tag{20}$$

At the instant of deposition the velocity gradient across the neutral cloud is equal to $1/\tau$ (see eq. (1)) and by virtue of assumption (4), that the velocity component of the ions in the direction of the magnetic field lines is the same as that of the parent neutral atom, it follows that the volume element in which the ions are deposited at instant τ will thereafter continue to elongate at a rate of $1/\tau$. Thus at epoch t the length of the unit volume (unit cross section and unit length) will have become

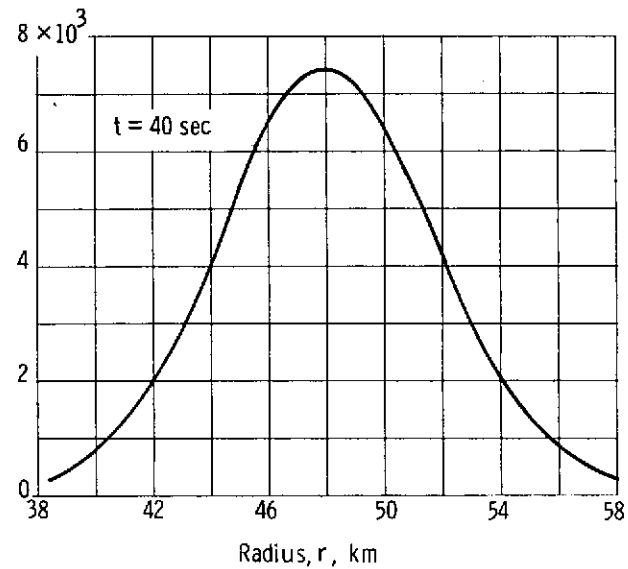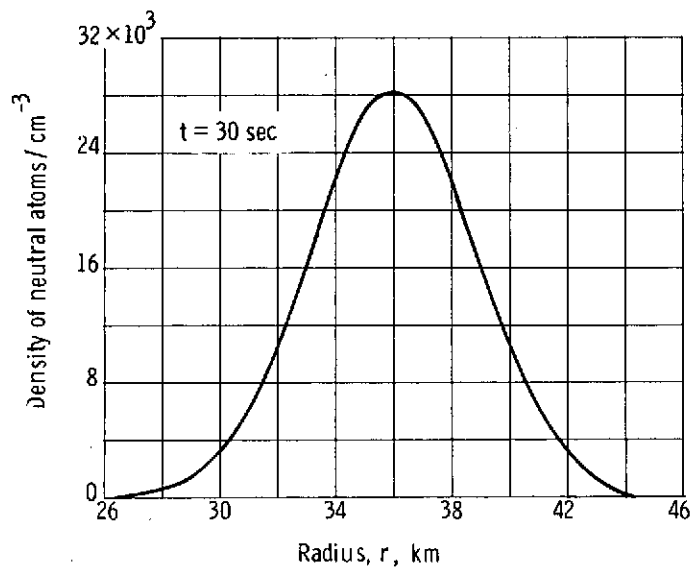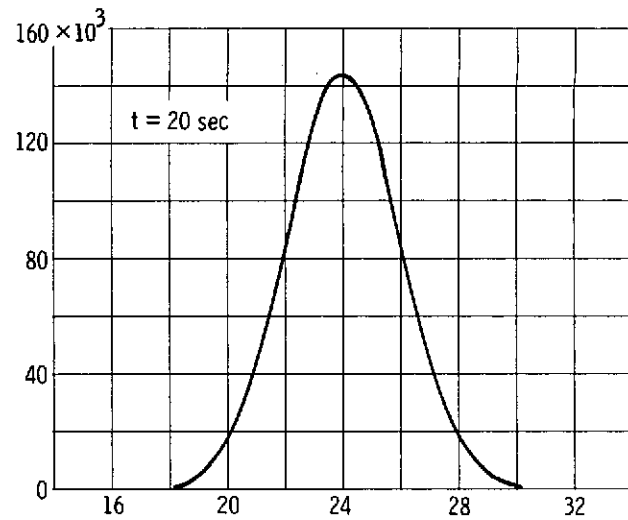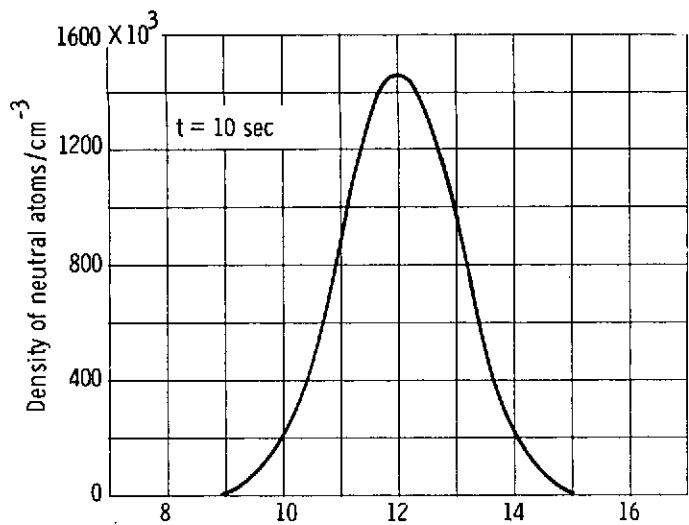$$1 + \frac{1}{\tau}(t - \tau) = \frac{t}{\tau}$$

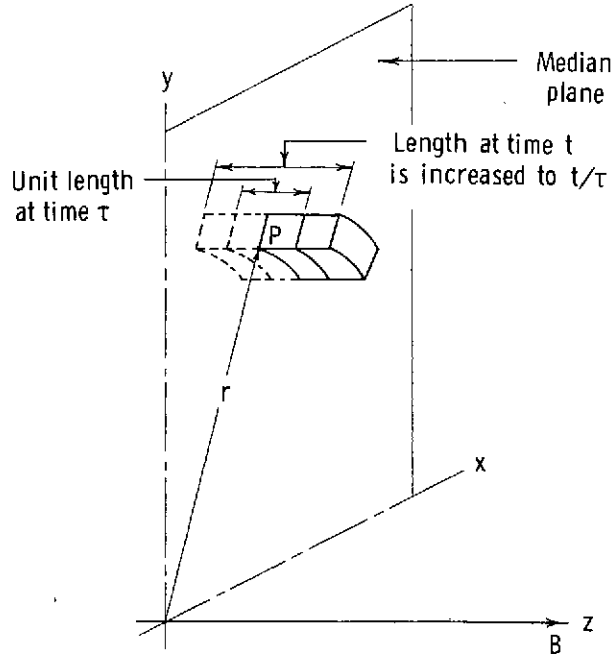Figure 7.- Radial density distribution of neutral barium atoms as function of time.

Figure 8.- Elongation of volume element with time.

and thus the ion density contributed at instant t by those ions formed during the interval τ to $\tau + \Delta\tau$ will be equal to

$$dn_i = \frac{\mu m c}{2fe^2\lambda\tau\frac{t}{\tau}}\left\{1 - \exp\left[-\frac{1}{\tau^2}\,G\!\left(\frac{r}{\tau},\tau\right)\right]\right\}d\tau \tag{21}$$

By integration the following expression for the density of ions in the median section at radius r at instant t is obtained

$$n_i(r,t) = \frac{\mu m c}{2fe^2\lambda t}\int_0^t\left\{1 - \exp\left[-\frac{1}{\tau^2}\,G\!\left(\frac{r}{\tau},\tau\right)\right]\right\}d\tau \tag{22}$$

Curves showing the variation of ion density with time at radii of 5, 10, and 15 km in the median section are plotted in figure 9. Note that the density at a given point remains small until the high-density portion of the neutral gas shell encroaches upon it. This is followed by a period of rapid buildup of ions as the dense shell passes over it, depositing ions as it does so. Once the dense portion of the neutral gas shell has passed by, there is a slow falloff in ion density as the ions disperse along the field lines. Figure 10 shows the radial ion distribution within the median section at epochs of 10, 20, and 40 seconds.
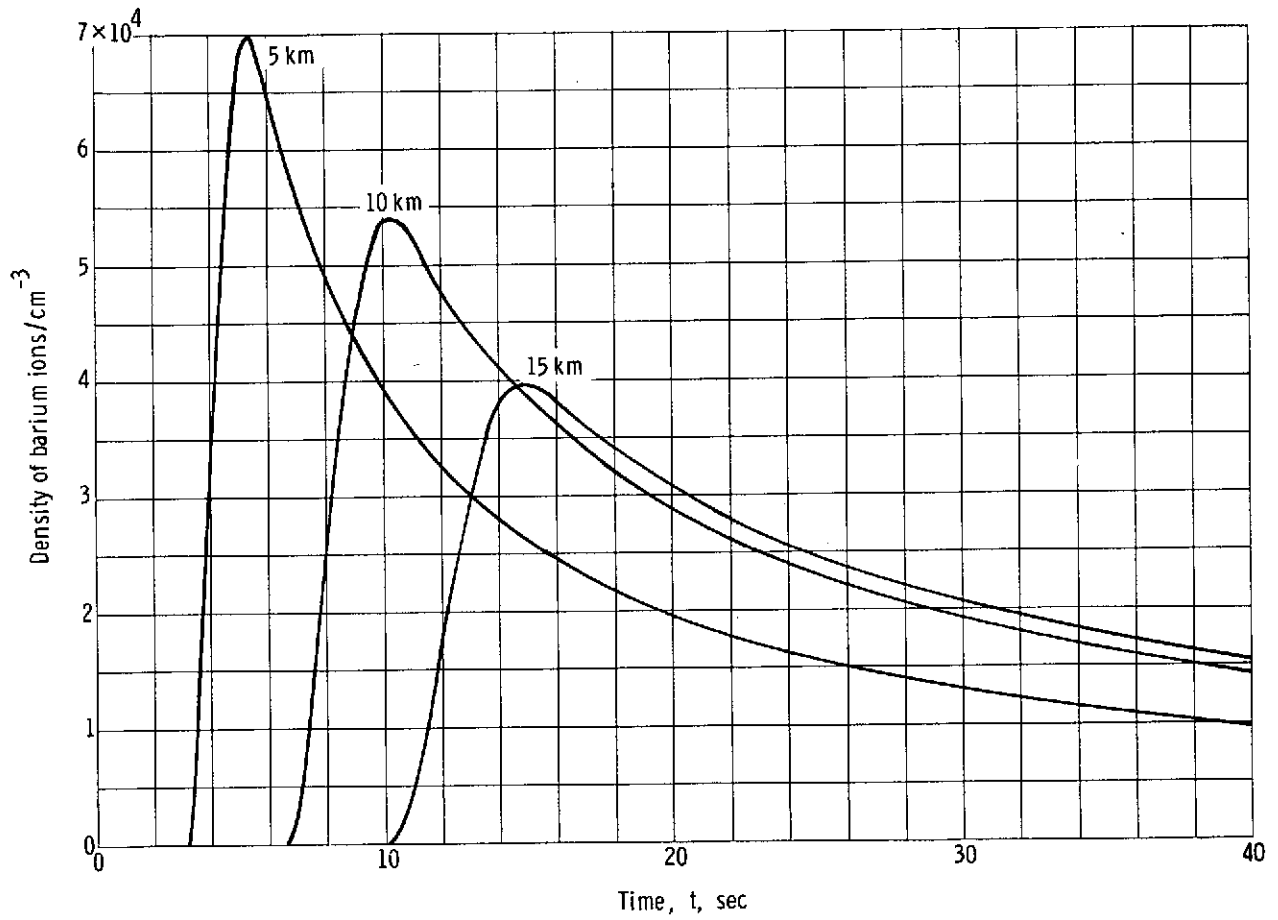
Figure 9.- Density of barium ions at selected radial distances in median cross section as function of time.
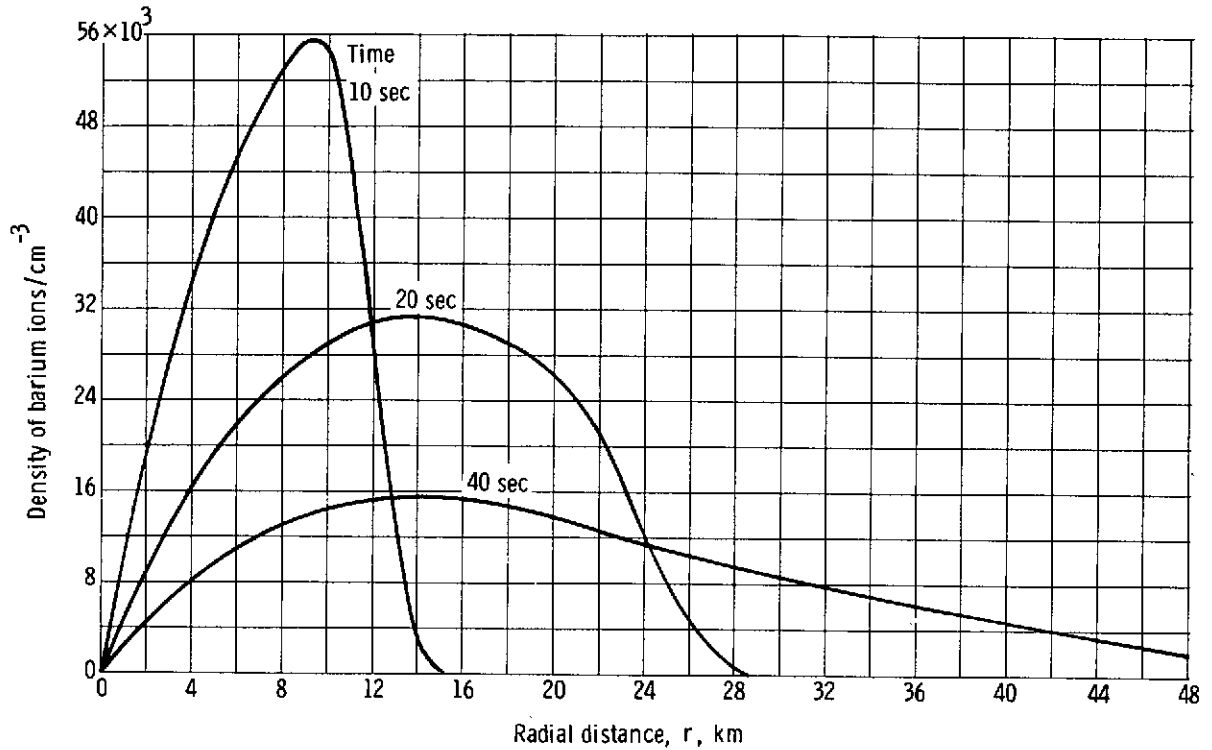
Figure 10.- Radial distribution of barium ions in median cross section
at selected epochs.

Brightness Variation Across Median Section of Ion Cloud

The brightness of an optically thin cloud is proportional to the number of ions within a column of unit cross-sectional area. By assuming the cloud to be viewed at instant t along a line of sight offset by a distance d from the cloud center (fig. 11), the brightness is given by

$$K \int_{-\infty}^{\infty} n_i\left(\sqrt{d^2 + x^2}, t\right) dx \tag{23}$$

where $n_i(r,t)$ is given by equation (22). Note that the integral in equation (23) defines the number of ions along a line perpendicular to the cloud axis. In the event the cloud is viewed obliquely, then the number of ions along the line of sight is equal to the integral (eq. (23)) multiplied by $\dfrac{1}{\sin \theta}$ where θ is the angle between the line of sight and the cloud centerline. This factor is assumed to have been absorbed in the constant K of equation (23).

The expression

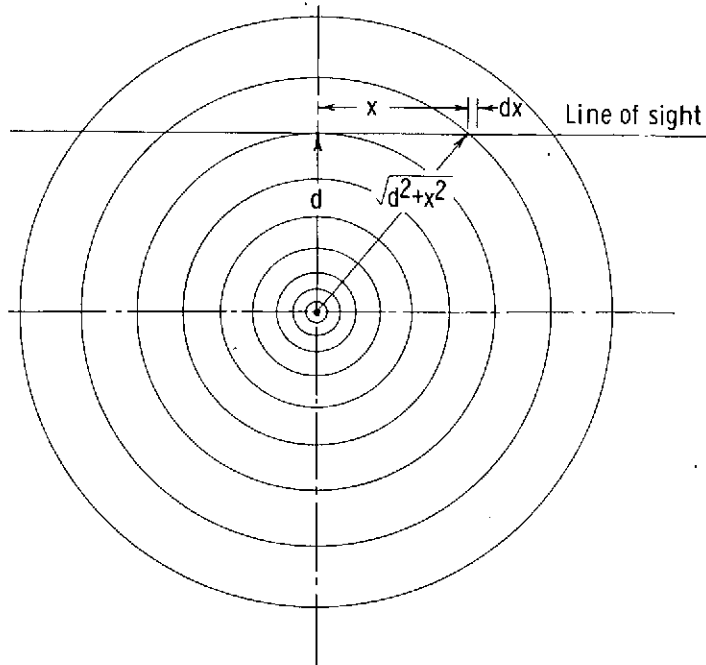$$\Phi = \int_{-\infty}^{\infty} n_i\left(\sqrt{d^2 + x^2}, t\right) dx$$

Figure 11.- Median cross section of ion cloud.

has been calculated as a function of ρ for the epochs of 10, 20, and 40 seconds following release. The results are presented in figure 12. Note the indentation of the brightness profile at early times in the proximity of the cloud axis. This could not be checked observationally because of obscuration of the ion cloud at early times by the superimposed neutral cloud.

DRIFT INSTABILITY

In the drift instability which leads to the formation of striations in ionospheric releases, an important role is played by the collisions taking place between drifting ions and background neutral particles, hence the name drift instability. There has been speculation that the same kind of instability may be operative at much higher altitudes, where the background density is virtually zero, by invoking collisions between outstreaming neutral barium atoms and the barium ions. Therefore a brief description of the instability and the reasons for rejecting it as a contributory cause of striation development in magnetospheric releases is given.

The underlying mechanism is illustrated in figure 13 depicting a cross section of the field-alined ion cloud relative to which the background neutrals are streaming from left to right (to an observer at rest relative to the neutral population, the cloud is drifting to the left and hence the forward and rearward faces are as indicated). If the magnetic field is
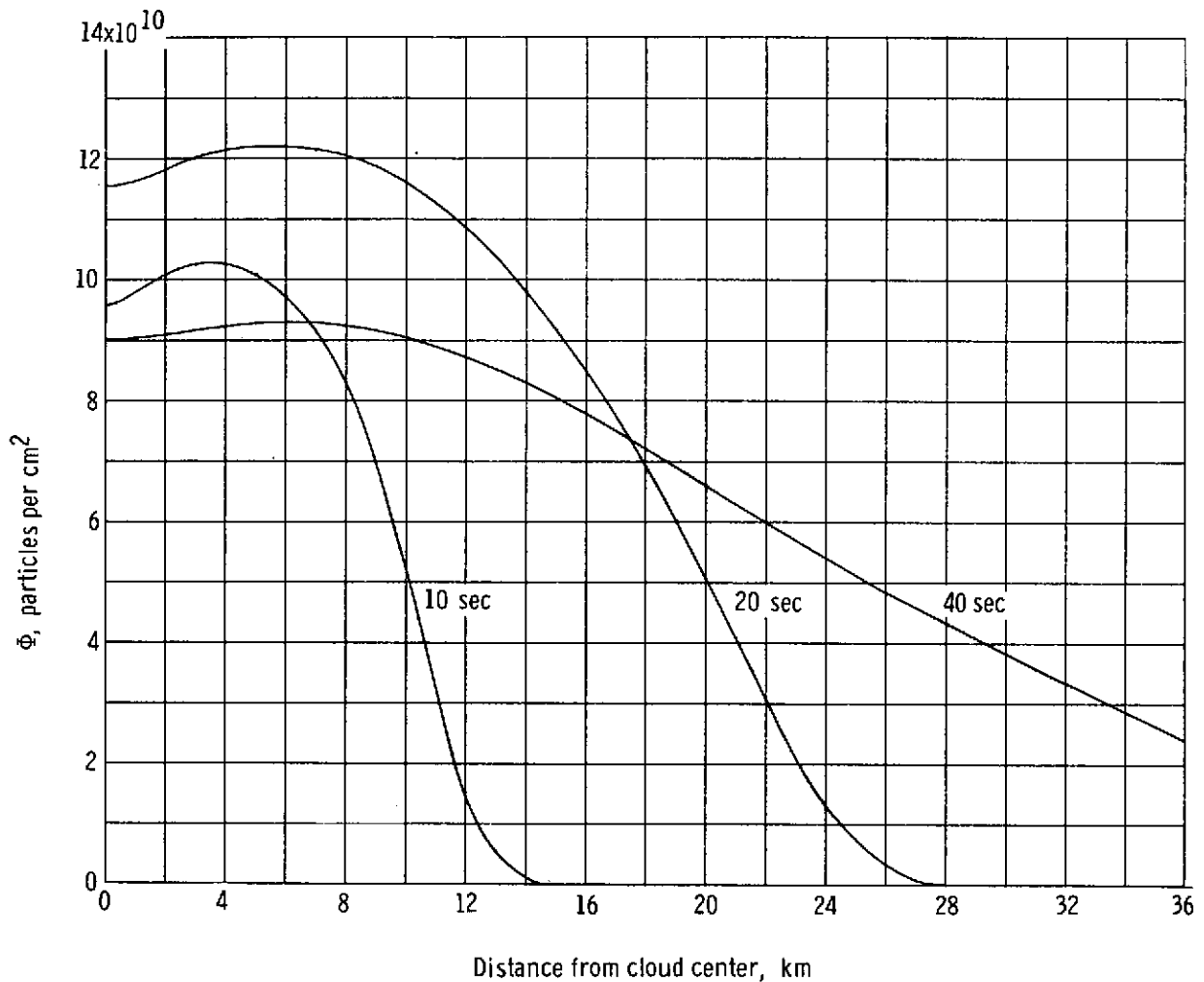
Figure 12.- Profile of brightness parameter Φ across median section of ion cloud.

assumed to be out of the plane of the paper, the drag force exerted by the neutrals on the charged particles will result in a drifting of positive ions and electrons in the downward and upward directions, respectively. If it is further supposed that the forward and rear-ward faces are rippled, as shown in figure 13, the accumulation of charge and the associated electric field $\vec{E}$ within the plasma will be in the direction depicted. Clearly, the polarization electric field causes the plasma to drift with velocity $\vec{E} \times \vec{B}/B^2$, which is in a direction to suppress the undulation on the forward face and to amplify it on the rear-ward face.

Turning now to a consideration of the barium releases in deep space, the ions as they form are constrained by the magnetic field and at early times there is a radial out-streaming of neutrals through them, as depicted in figure 14. Clearly, the conditions existing at the surface of the ion cloud correspond to those prevailing at the rearward
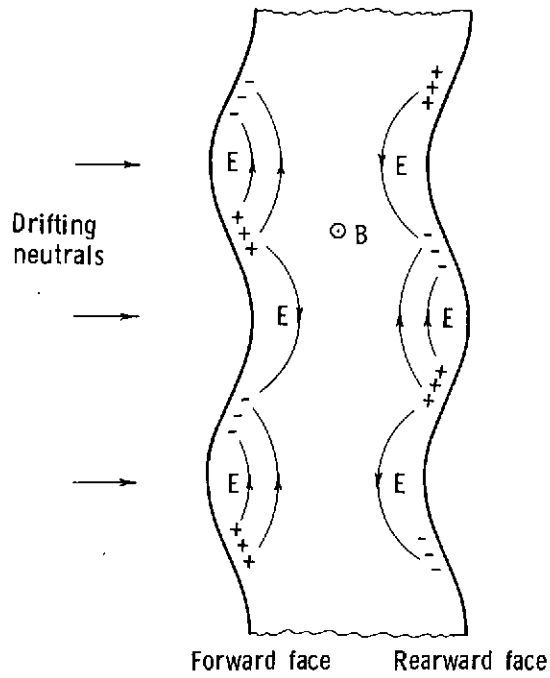
24

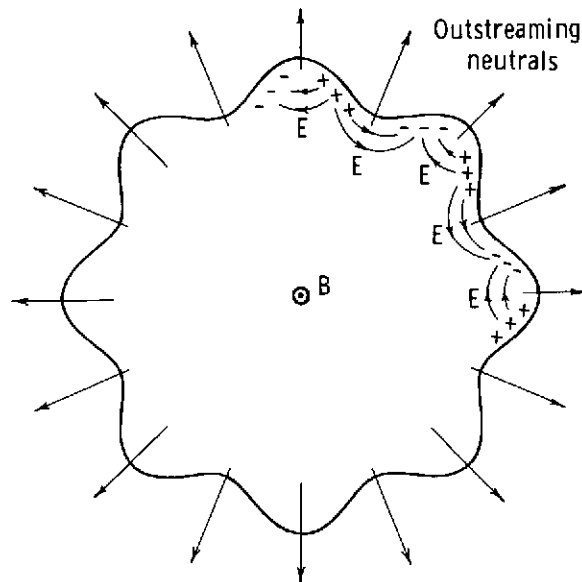Figure 13.- Cross section of ion cloud released in ionosphere.

Figure 14.- Cross section of ion cloud released in deep space.

face of the ionospheric cloud in the previous example (fig. 13). Conditions are, therefore, conducive to instability.

By using the results of the analysis of the preceding section, a plot has been made of peak neutral density as a function of time (fig. 15). By adopting a collisional cross-sectional radius of 6 Å for encounters between neutral barium atoms and barium ions, the interval between successive encounters of an ion with neutrals is given as a function of time in figure 16. Note that at 1.5 seconds after release the interval between collisions is 2.0 seconds, and after 5 seconds the collisional interval has increased to about 75 seconds. Obviously collisions between ions and neutrals can be ignored after several seconds. However, referring to figure 6, note that too few ions are formed within the collision-dominated phase of the cloud expansion to support the type of instability under discussion.
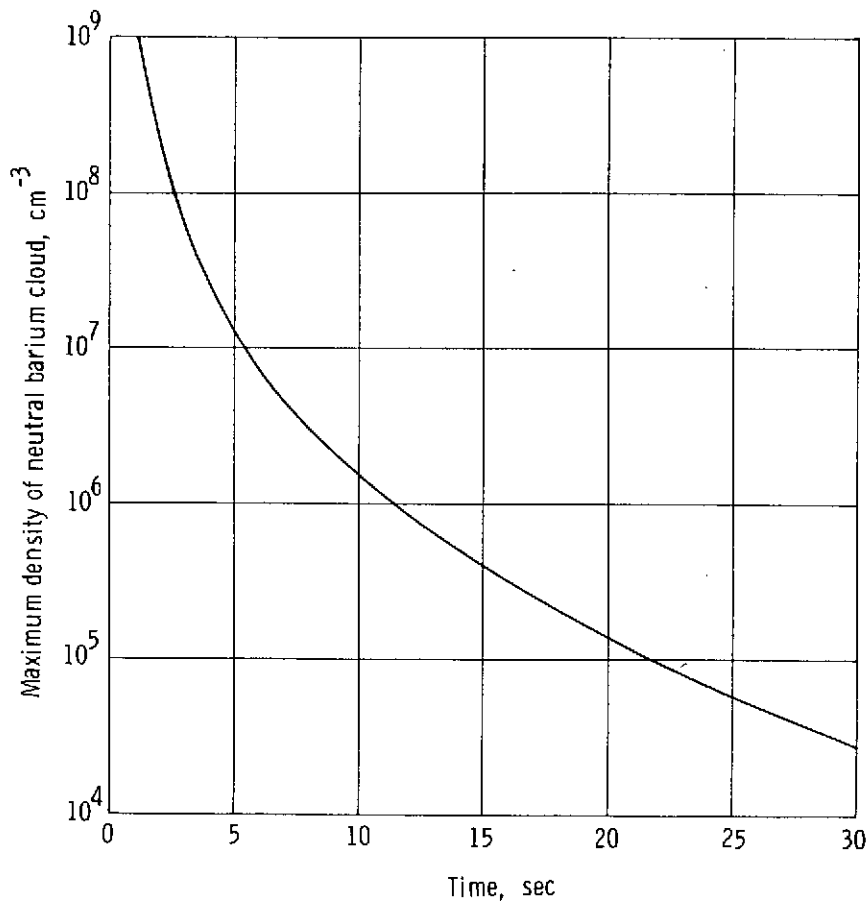

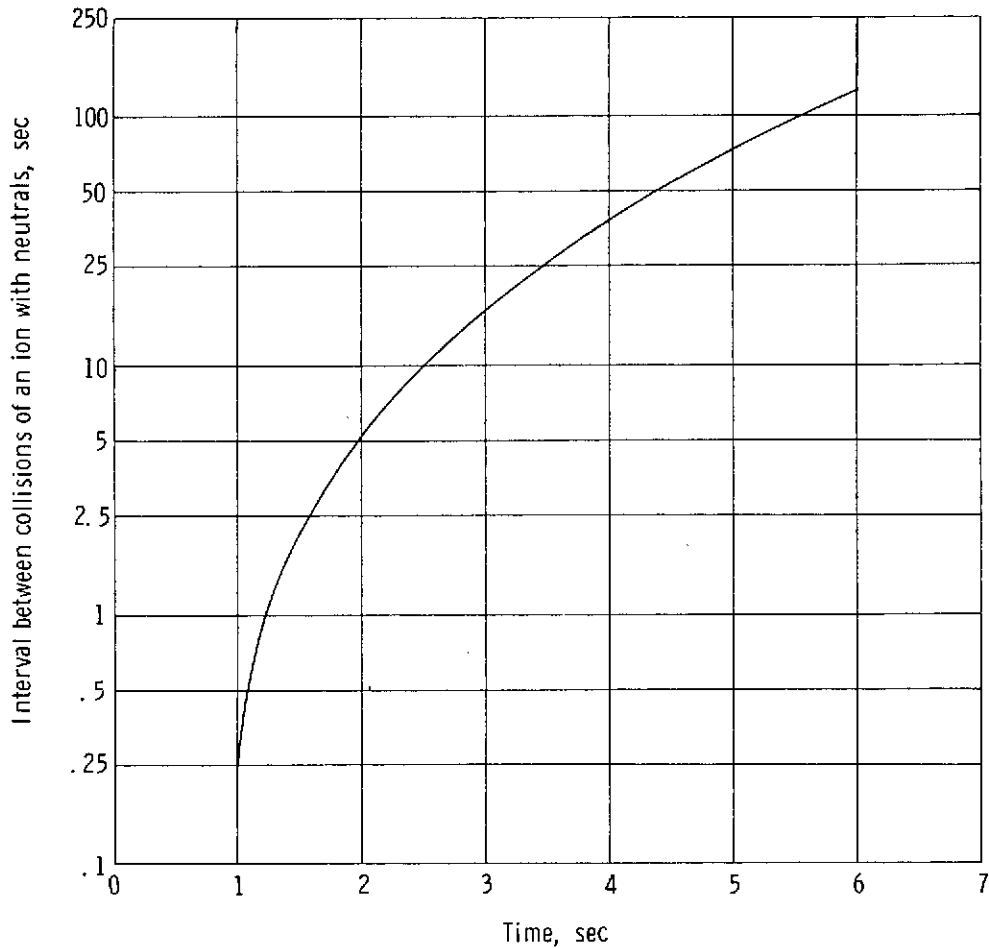Figure 15.- Maximum density of neutral cloud as function of time.

Figure 16.- Interval between collisions of an ion with neutrals as function of time.

RAYLEIGH-TAYLOR AND FLUTE INSTABILITIES

In the present section the assumption is made that the rapid formation of the ion cloud in the weak magnetic field existing at 5 Earth radii results in a thrusting apart of the magnetic field lines. Thus, whereas the cloud elongation in the direction of the magnetic field proceeds without impediment, its transverse expansion is opposed by an inwardly directed magnetic pressure. During the resulting radial deceleration the inertial forces on the plasma are outwards. The situation is clearly analogous to one in which a heavy fluid is supported by one of zero density in a gravitational field, and the cloud boundary is therefore prone to the so-called Rayleigh-Taylor instability. In addition, the configuration is subject to flute instabilities of the kind discussed in reference 18. Thus, suppose that the cloud boundary becomes fluted, as shown in figure 17, and that the magnetic field is wholly excluded from the cloud interior, then the integral of the magnetic field vector taken around a circuit extending from a to b along a crest (solid line in fig. 17) and from b to a along an adjacent trough (dashed line in fig. 17) is zero since no current is threading the
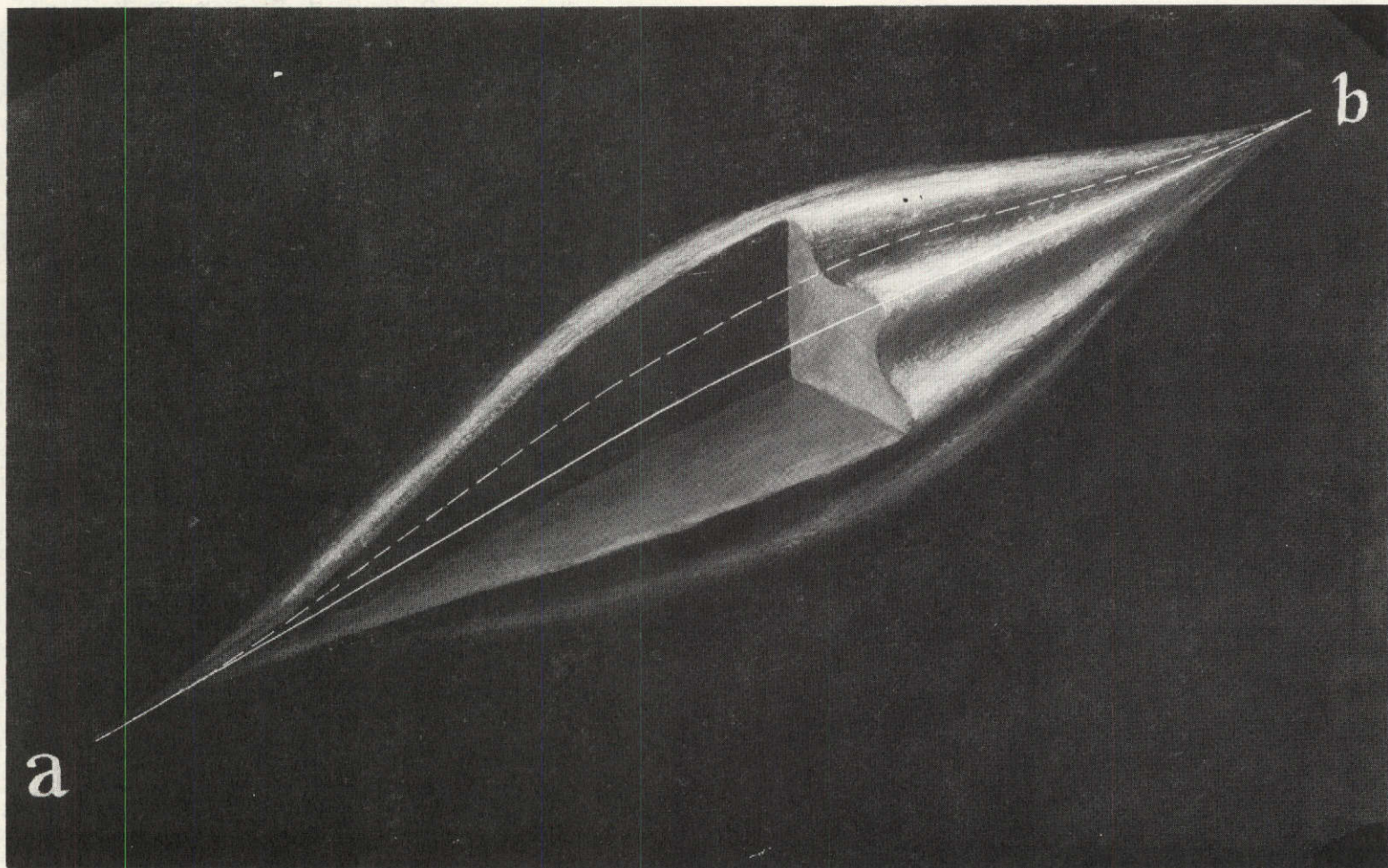
27

Figure 17.- Ion cloud with fluted boundary.

circuit. It follows therefore that since the arc length along a crest exceeds that along a trough, the magnetic field pressure at a crest is less than that at a trough, a condition conducive to further growth of the flutes. Both of these instabilities, Rayleigh-Taylor and flute, are quantitatively analyzed in this section. The general approach used has similarities with that adopted in reference 8, however the manner of derivation as herein presented differs from that of the aforementioned reference as do the end results.

Analysis

By introducing cylindrical coordinates, the axisymmetric unperturbed boundary is given by the expression $r = r(z,t)$. In the stability analysis consideration is limited to motion in the equatorial (median) plane. Denote the unperturbed equatorial radius of the ion cloud boundary by r_m, which is a function of time t, and denote the radial distance from the unperturbed boundary by η measured positive outwards. The equation of motion in the radial direction is given by

$$\rho \frac{d^2}{dt^2}\left(r_m + \eta\right) = -\nabla_\eta (p) + \left(\vec{j} \times \vec{B}\right)_\eta$$

$$\rho \frac{d^2 \eta}{dt^2} = -\nabla_\eta (p) + \rho g + \left(\vec{j} \times \vec{B}\right)_\eta \tag{24}$$

where

$$g = -\frac{d^2 r_m}{dt^2}$$

In the magnetohydrodynamic approximation, which is used throughout

$$\vec{j} = \frac{1}{\mu_o} \nabla \times \vec{B}$$

Thus

$$\vec{j} \times \vec{B} = -\frac{1}{\mu_o} \vec{B} \times \left(\nabla \times \vec{B}\right) = -\nabla\left(\frac{B^2}{2\mu_o}\right) + \frac{1}{\mu_o}\left(\vec{B} \cdot \nabla\right)\vec{B} \tag{25}$$

If $\vec{b}$ denotes the unit vector in the direction of the magnetic field, then the operator $\vec{b} \cdot \nabla\left(\equiv \frac{\partial}{\partial s}\right)$ denotes differentiation along the magnetic field lines. Bearing in mind that in the proximity of the median plane the magnitude of the magnetic field is constant to a first order, it follows from figure 18 that

$$\left(\vec{B} \cdot \nabla\right)\vec{B} = B\frac{\partial \vec{B}}{\partial s} = -B^2\frac{\vec{R}}{R} \tag{26}$$

where $\vec{R}$ is the radius of curvature vector of the magnetic field lines.
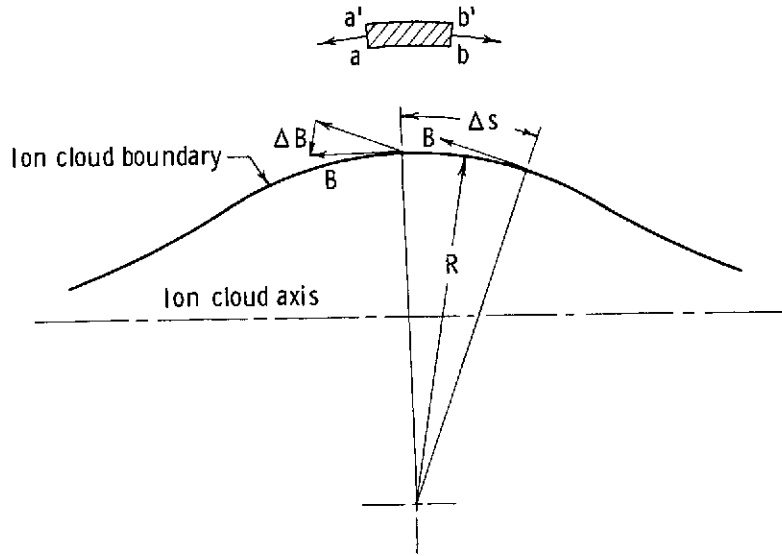
Figure 18.- Cross section through ion cloud axis.

As stated previously, at very early times prior to striation formation exclusion of magnetic field lines from the ion cloud interior would be expected. If this is assumed to be true, then equation (24) becomes

$$\rho \frac{d^2 \eta}{dt^2} = -\frac{\partial p}{\partial \eta} + \rho g \tag{27}$$

External to the barium cloud the ambient plasma pressure and density are to all intents and purposes zero. Bearing this in mind and substituting equations (25) and (26) into equation (24)

$$0 = -\frac{\partial}{\partial \eta}\left(\frac{B_e^2}{2\mu_o}\right) - \frac{B_e^2}{\mu_o R} \tag{28}$$

where B_e denotes the magnetic field exterior to the cloud.

Equation (28) expresses the balance of forces acting on the magnetic tube segment aa'bb' in figure 18. The inward force $-\dfrac{B_e^2}{\mu_o R}$ results from the tensions acting at the ends aa' and bb', and the outward force $-\dfrac{\partial}{\partial \eta}\left(\dfrac{B_e^2}{2\mu_o}\right)$ results from the compressive pressure exerted by contiguous magnetic tubes across the lateral faces ab and a'b'.

When the values of the unperturbed parameters are denoted by the addition of a tilde over the appropriate symbol, the unperturbed pressure is denoted $\tilde{p}(\eta,t)$, and so forth. With this notation equations (27) and (28) become

$$\tilde{p} = \tilde{p}_o + \rho g \eta \tag{29}$$

where the subscript o corresponds to the location of the unperturbed boundary, that is, $\eta = o$, and

$$\frac{\partial}{\partial \eta}\left(\frac{\tilde{B}_e^2}{2\mu_o}\right) + \frac{\tilde{B}_e^2}{\mu_o R} = 0 \tag{30}$$

The pressure balance at the unperturbed boundary further requires

$$\tilde{p}_o = \left(\frac{\tilde{B}_e^2}{2\mu_o}\right)_o \tag{31}$$

Now assume a perturbation of the boundary having the form of magnetic field-alined ripples as shown in figure 17. Thus, the perturbed boundary in the equatorial plane is given by the expression

$$\eta = \delta\eta e^{iq\phi} \tag{32}$$

where ϕ is the azimuthal angle.

Figure 19 depicts the boundary distortion in the equatorial plane for the mode $q = 8$. The circumferential wavelength of the fluting is given by $\lambda_c = \frac{2\pi r_m}{q}$. The corresponding wave number is given by

$$k = \frac{2\pi}{\lambda_c} = \frac{q}{r_m} \tag{33}$$

The perturbation to a field quantity P associated with the boundary perturbation has the form

$$\left.\begin{array}{ll}\delta(P) \propto e^{-k\eta}e^{iq\phi} & \text{(outside the boundary)} \\[2ex] \delta(P) \propto e^{k\eta}e^{iq\phi} & \text{(inside the boundary)}\end{array}\right\} \tag{34}$$

where the sign of the exponent defining the radial dependence of the perturbation is so chosen to ensure an exponential falloff in the perturbation away from the boundary in either direction. Specifically
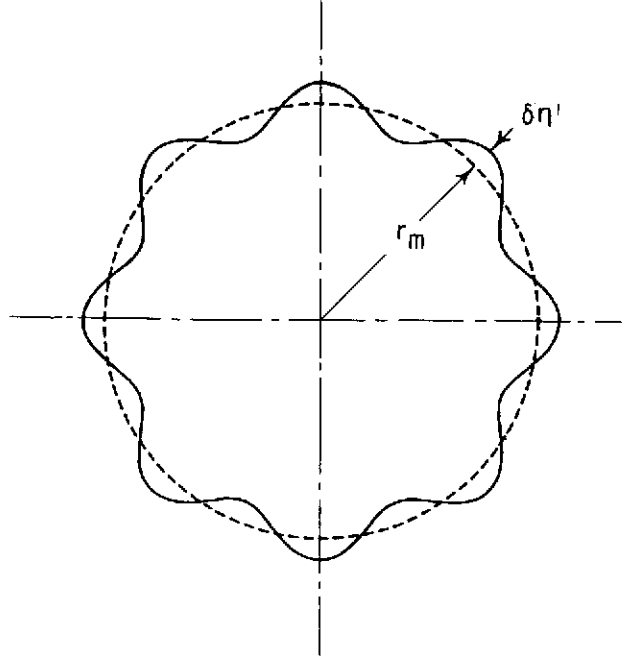
31

Figure 19.- Equatorial boundary perturbation (q = 8).

$$\left.\begin{array}{l} p = \tilde{p}_o + \rho g \eta + \delta p e^{k \eta} e^{i q \phi} \\[3mm] \dfrac{B_e^{~2}}{2 \mu_o} = \dfrac{\tilde{B}_e^{~2}}{2 \mu_o} + \delta \left(\dfrac{B_e^{~2}}{2 \mu_o}\right) e^{-k \eta} e^{i q \phi} \\[3mm] \dfrac{B_e^{~2}}{\mu_o R} = \dfrac{\tilde{B}_e^{~2}}{\mu_o R} + \delta \left(\dfrac{B_e^{~2}}{\mu_o R}\right) e^{-k \eta} e^{i q \phi} \end{array}\right\} \qquad (35)$$

The radial motion of a plasma element contiguous to, and inside the boundary, will necessarily be the same as that of the boundary. By substituting equations (32) and (35) into equation (27)

$$\rho \frac{d^2 (\delta \eta)}{dt^2} e^{i q \phi} = -\frac{\partial}{\partial \eta} \left(\tilde{p}_o + \rho g \eta + \delta p e^{k \eta} e^{i q \phi}\right) + \rho g$$

Thus

$$\rho \frac{d^2 (\delta \eta)}{dt^2} = -k \delta p \qquad (36)$$

By substituting equation (35) into equation (28) and subtracting equation (30) to first order

32

$$k\delta\left(\frac{B_e^2}{2\mu_o}\right) - \delta\left(\frac{B_e^2}{\mu_o R}\right) = 0 \tag{37}$$

The pressure balance at the perturbed interface requires that at $\eta = \delta\eta e^{iq\phi}$

$$\tilde{P}_o + \rho g\eta + \delta p e^{k\eta} e^{iq\phi} = \left(\frac{\tilde{B}_e^2}{2\mu_o}\right)_o + \eta\left[\frac{\partial}{\partial\eta}\left(\frac{\tilde{B}_e^2}{2\mu_o}\right)\right]_o + \delta\left(\frac{B_e^2}{2\mu_o}\right)e^{-k\eta}e^{iq\phi}$$

By substituting equation (31) and retaining only terms of first order

$$\rho g\delta\eta + \delta p = \delta\eta\left[\frac{\partial}{\partial\eta}\left(\frac{\tilde{B}_e^2}{2\mu_o}\right)\right]_o + \delta\left(\frac{B_e^2}{2\mu_o}\right) \tag{38}$$

By using equation (28), equation (38) can be rewritten as

$$\delta p = -\rho g\delta\eta - \frac{\tilde{B}_{e_o}^2}{\mu_o R_o}\delta\eta + \delta\left(\frac{B_e^2}{2\mu_o}\right) \tag{39}$$

By assuming the diamagnetic plasma cloud to have the spindle shape depicted in figure 20, then for this case from equations (36) and (39)

$$\rho\frac{d^2(\delta\eta)}{dt^2} = k\left(\rho g + \frac{\tilde{B}_{e_o}^2}{\mu_o R_o}\right)\delta\eta - k\frac{B_e\delta B_e}{\mu_o} \tag{40}$$
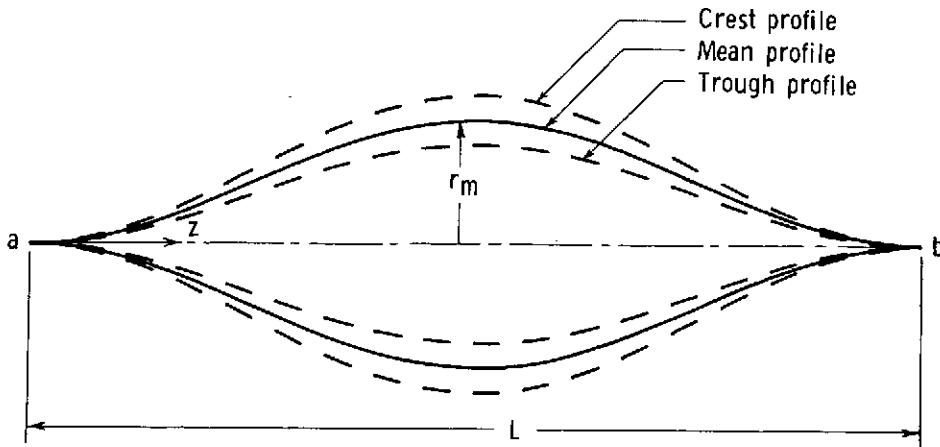

Figure 20.- Longitudinal cross section of ion cloud.

From Longmire (ref. 19)

$$\frac{\delta B_e}{B_e} = -\frac{\delta l}{l} \tag{41}$$

where

δB_e perturbation in magnetic field at crest in equatorial plane

δl amount by which length of crest profile exceeds undeformed profile

By assuming the equation of the undeformed profile to be

$$r = \frac{r_m}{2}\left(1 - \cos\frac{2\pi z}{L}\right) \tag{42}$$

its profile arc length measured between points a and b (fig. 20) is given by

$$l = \int_0^L \sqrt{1 + \left(\frac{dr}{dz}\right)^2}\,dz \tag{43}$$

For the crest profile

$$r + dr = (1 + \epsilon)\frac{r_m}{2}\left(1 - \cos\frac{2\pi z}{L}\right) \tag{44}$$

and its arc length between points a and b is therefore

$$
\begin{aligned}
l + dl &= \int_0^L \sqrt{1 + (1 + \epsilon)^2\left(\frac{dr}{dz}\right)^2}\,dz \\
&= \int_0^L \sqrt{1 + \left(\frac{dr}{dz}\right)^2}\,dz + \epsilon \int_0^L \frac{\left(\frac{dr}{dz}\right)^2}{\sqrt{1 + \left(\frac{dr}{dz}\right)^2}}\,dz
\end{aligned}
\tag{45}
$$

From equations (43) and (45) and by assuming the cloud profile to be reasonably slender

$$dl \approx \epsilon \int_0^L \left(\frac{dr}{dz}\right)^2\,dz$$

By substituting equation (42)

$$dl \approx \epsilon\left(\frac{\pi r_m}{L}\right)^2 \int_0^L \sin^2\left(\frac{2\pi z}{L}\right)\,dz$$

Hence

$$\frac{dl}{l} \approx \frac{\epsilon}{2}\left(\frac{\pi r_m}{L}\right)^2 \tag{46}$$

Moreover

$$\frac{1}{R_o} = -\left(\frac{d^2 r}{dz^2}\right)_{z=\frac{L}{2}} = \frac{2\pi^2 r_m}{L^2} \tag{47}$$

By substituting equations (41), (46), and (47) into equation (40) and bearing in mind that $\delta\eta = \epsilon r_m$

$$\rho \frac{d^2(\delta\eta)}{dt^2} = k\left(\rho g + \frac{5}{2}\frac{\pi^2}{\mu_o}\frac{B_e^2 r_m}{L^2}\right)\delta\eta$$

By assuming an exponential growth of the instability $\delta\eta \propto e^{\alpha t}$ and substituting expression (33) for k, the dispersion relation becomes

$$\alpha = \sqrt{q\left(\frac{g}{r_m} + \frac{5}{2}\frac{\pi^2}{\mu_o}\frac{B_e^2}{\rho L^2}\right)} \tag{48}$$

This relation implies that the exponential growth rate increases without bound as q increases. This, however, is physically unrealistic. Remember that the ions can move to and fro within the field free cloud interior, and therefore their thermal motion will tend to erode the crests and fill in the hollows of the fluted boundary. The time taken by an average ion to move from a crest to a hollow as a result of thermal motion is clearly

$$\tau_d = \frac{\pi r_m}{q v_{th}} \tag{49}$$

In the absence of instabilities a subsidence of flutes resulting from thermal agitation as given by the expression $e^{-\kappa t/\tau_d}$ where κ is a numerical factor might be expected. The net growth rate is thus given by

$$e^{\bar{\alpha} t} = e^{\alpha t} e^{-\kappa t/\tau_d}$$

Thus

$$\bar{\alpha} = \sqrt{q\left(\frac{g}{r_m} + \frac{5}{2}\frac{\pi^2}{\mu_o}\frac{B_e^2}{\rho L^2}\right)} - \frac{\kappa q v_{th}}{\pi r_m} \tag{50}$$

For sufficiently small wavelengths (large enough q) the exponent $\bar{\alpha}$ becomes negative and the flutes are eroded more rapidly than they can amplify through inherent instability. Thus, in this case, thermal agitation of the ions quenches the instability.

For convenience introduce

$$\beta = \frac{g}{r_m} + \frac{5}{2} \frac{\pi^2}{\mu_0} \frac{B_e^2}{\rho L^2} \tag{51}$$

Hence

$$\bar{\alpha} = \sqrt{q\beta} - \frac{\kappa q v_{th}}{\pi r_m} \tag{52}$$

The mode of deformation subject to greatest growth rate is obtained from the equation

$$\frac{d\bar{\alpha}}{dq} = \frac{1}{2}\sqrt{\frac{\beta}{q}} - \frac{\kappa v_{th}}{\pi r_m} = 0$$

$$q = \frac{\pi^2 \beta r_m^2}{4\kappa^2 v_{th}^2} \tag{53}$$

and the corresponding maximum growth rate is given by

$$\bar{\alpha}_{max} = \frac{\pi \beta r_m}{4\kappa v_{th}} \tag{54}$$

This analysis is based on the premise that there is complete exclusion of magnetic field from the cloud interior. This is at variance with the assumption invoked in the analysis of cloud evolution given in a previous section. The true answer lies somewhere between. Numerical simulations of cloud release and ionization described in reference 15 support the contention that there is complete exclusion from the inner core of the ion cloud; however, in these numerical studies the condition of radial symmetry was enforced and no allowance was made for three-dimensional effects. The presence of a magnetic field in the cloud interior would not be expected to influence markedly the contribution of the Rayleigh-Taylor-type of instability; however, it would increase the growth time of the flute-type instability. In addition, the reduced constraint on cloud expansion would reduce the effective acceleration g and an interior field would inhibit thermal motion of the ions, thus modifying the damping factor. The net result of all of these competing effects is difficult to predict.

The buildup of electron charges on the faces of the surface flutes gives rise to polarization electric fields within the cloud interior. These electric fields propagate downwards along the magnetic field lines at Alfvén velocity and are shorted out at ionospheric levels where the Pederson conductivity is large. In the context of ionospheric releases these effects result in a partial quenching of the instabilities (ref. 4). For the barium release at 31 500 km there is a lapse of about 25 seconds before the polarization field manifests itself at ionospheric levels. Bearing in mind the rapid growth of the instabilities indicated by both observation and results of numerical studies given in the following subsection, the time of about 50 seconds before such ionospheric perturbations can rebound to the cloud is too long to exert any significant influence.

Applications to Barium Ion Cloud Release at 31 500 km

If complete exclusion of magnetic field lines from the cloud core is assumed, then to achieve a pressure balance at the core boundary

$$\frac{B^2}{2\mu_0} = n_e kT \tag{55}$$

where

B   ambient magnetic field strength $\left(150 \text{ gamma} = 15 \times 10^{-8} \text{ tesla}\right)$

$\mu_0 = 4\pi \times 10^{-7}$ H/m

n_e equilibrium ion density

k   Boltzmann constant

T   initial ion cloud temperature (4000 K)

Thus, from equation (55) an equilibrium ion density of $n_e = 1.63 \times 10^{11}$ ions/m^3 is obtained.

The initial rate of increase of cloud length between half-brightness points is given in reference 9 as 1400 m/sec. The overall rate of elongation might be expected to be about twice as great. Thus, by using subscript e to denote values at the instant of pressure equalization

$$L_e(\text{meters}) = 2800t_e \tag{56}$$

The initial rate of radial expansion of the ions may plausibly be taken equal to the mean radial velocity of the parent neutral atoms (1200 m/sec). This radial velocity drops to zero as equilibrium is approached. Thus, the rate of radial expansion averaged over the entire deceleration period is 600 m/sec, and

$$r_e \text{(meters)} = 600 t_e \tag{57}$$

The total barium yield is estimated to have been 1.7 kg $\left(N(0) = 7.45 \times 10^{24} \text{ barium atoms} \right)$. If the ion cloud is assumed to have the form of a prolate spheroid and the number of ions to be given by the simple relation $N_i(t) = N(0)\left(1 - e^{-0.05t} \right)$, then at the instant of pressure equalization

$$\frac{2}{3} \pi r_e^2 L_e n_e = \left(1 - e^{-0.05t_e} \right) 7.45 \times 10^{24} \tag{58}$$

By substituting the value $n_e = 1.63 \times 10^{11}$ ions/m^3 and equations (56) and (57) into equation (58), the following equation is obtained

$$\frac{t_e^3}{1 - e^{-0.05t_e}} = 2.16 \times 10^4$$

From this equation a deceleration time of 25 seconds is computed. Hence, the cloud length at midpoint of deceleration phase is $L = 2800 \times 12.5 = 35\,000$ m.

By taking $v_o = 1200$ m/sec and $r_e = 600 \times 25 = 15\,000$ m, for the effective cloud deceleration

$$g = \frac{v_o^2}{2 r_e} = 48 \text{ m/sec}^2$$

Thus, the cloud radius at epoch t is given by

$$r = v_o t - \frac{1}{2} g t^2$$

and the cloud radius at midpoint of deceleration phase is

$$r_m = 11\,200 \text{ m}$$

By introducing these numerical values into equation (51)

$$\beta = 14.1 \times 10^{-3} \text{ sec}^{-2}$$

The mean ion velocity v_{th}, corresponding to an initial ion cloud temperature of 4000 K, is equal to 900 m/sec. By using these values in equation (53), the equation obtained for the harmonic mode most susceptible to instability is

$$q = \frac{5.38}{\kappa^2} \tag{59}$$

The exponential growth time associated with this most unstable mode is from equation (54) equal to 7.3κ seconds. In figure 2(b) about 10 prominent striational features can be discerned. Setting $q = 10$ in equation (59) yields $\kappa = 0.74$ and an exponential growth time of about 5.3 seconds.

From equation (52) the variation in exponential growth time $\bar{\alpha}^{-1}$ with harmonic mode of azimuthal perturbation q is determined. The results are plotted in figure 21 for $\kappa = 0.74$.
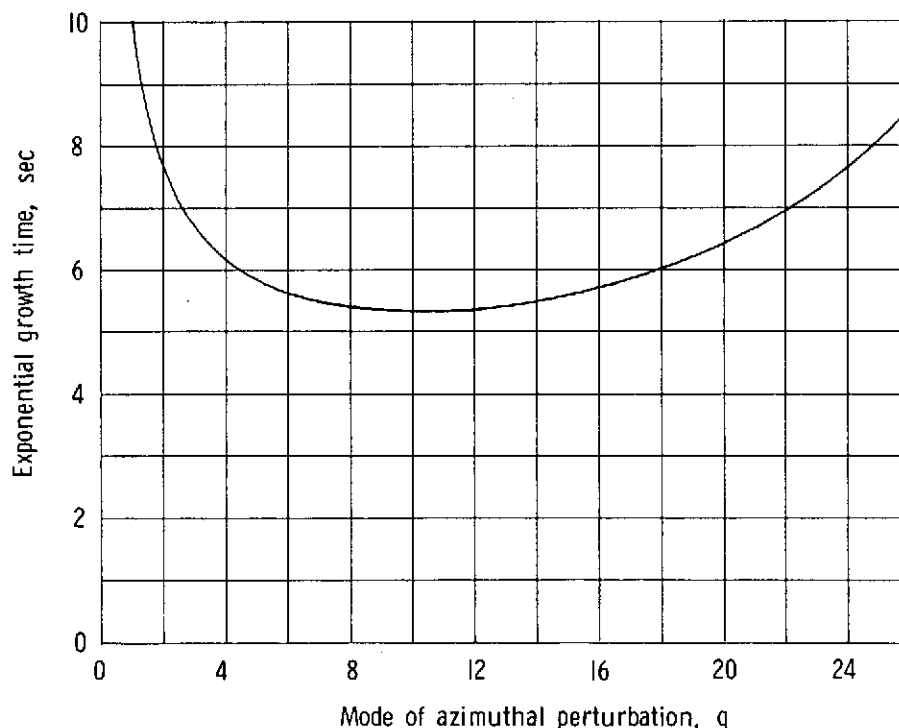

Figure 21.- Exponential growth time as function of mode of azimuthal perturbation.

CONCLUDING REMARKS

The regularity of the striational features observed in the barium ion cloud (BIC) release on September 1971 precludes their being attributed to the delineation of field-alined inhomogeneities preexisting the release. The observational data further indicate that the striations did form at early times, presumably during the transient phase of cloud formation.

Throughout the initial phase of cloud evolution there is a radial outstreaming of neutral atoms through the ions, which have been formed and are constrained by the permeating magnetic field. The conditions prevailing at the ion cloud boundary are thus quite similar to those existing at the rearward face of ion clouds formed at ionospheric altitudes and drifting with respect to the background neutral atmosphere. For the ionospheric release these conditions are conducive to the onset of drift instability and are believed to play an important part in striation formation. The possible role played by drift instability in formation of striations in magnetospheric releases has been examined. The ion density is too low during the collision-dominated phase of cloud expansion to support an instability of this kind.

The other instability investigated in the present paper, the so-called Rayleigh-Taylor flute instability, is believed to explain plausibly the striational structure observed in the BIC experiment, both with regard to number of striations formed and their formation rates. Essentially the same instability had been invoked by Pilipp to explain the formation of some tenuous striations in an earlier magnetospheric release of March 18, 1969. Although there appears to be agreement regarding the basic mechanism of instability, the analytical treatment presented herein and the dispersion relation describing the instability growth differ from those of Pilipp.

The question as to whether there is exclusion of magnetic field lines from the ion cloud interior during its expansion remains an open one. In the present paper two contrary viewpoints have been adopted; thus in the treatment of ion cloud formation and the drift instability it has been assumed that there is no distension of the magnetic field during the ion deposition, whereas in the discussion of the Rayleigh-Taylor flute instability it has been assumed that there is complete magnetic field exclusion from the ion cloud interior. The true answer probably lies somewhere in between.

The destabilizing mechanism proposed for the striation formation in the present experiment would presumably be operative at times of sudden injection of plasma into the inner magnetosphere during geomagnetic storms. This may well contribute in part to the formation of those field-alined inhomogeneities in the magnetosphere which serve as

whistler ducts. In this connection it would be of interest to determine whether the number of whistler ducts tends to correlate with geomagnetic storms.

Langley Research Center,
National Aeronautics and Space Administration,
Hampton, Va., July 1, 1974.

REFERENCES

1. Westcott, Eugene M.; Heppner, James P.; Stolarick, John D.; Hallinan, Thomas; Davis, T. Neil; and Romick, G. J.: Rapid Ray Motions Through Barium Ion Clouds and Associated Auroras. Trans., Amer. Geophys. Union (Abstr. STM 32), vol. 50, no. 4, Apr. 1969, p. 281.

2. Linson, Lewis M.; and Workman, Joseph B.: Formation of Striations in Ionospheric Plasma Clouds. J. Geophys. Res., vol. 75, no. 16, June 1, 1970, pp. 3211-3219.

3. Simon, Albert: Growth and Stability of Artificial Ion Clouds in the Ionosphere. J. Geophys. Res., vol. 75, no. 31, Nov. 1, 1970, pp. 6287-6294.

4. Völk, Heinrich J.; and Haerendel, Gerhard: Striations in Ionospheric Barium Clouds. 1. J. Geophys. Res., vol. 76, no. 19, July 1, 1971, pp. 4541-4559.

5. Perkins, F. W.; Zabusky, N. J.; and Doles, J. H., III: Deformation and Striation of Plasma Clouds in the Ionosphere. 1. J. Geophys. Res., vol. 78, no. 4, Feb. 1, 1973, pp. 697-709.

6. Zabusky, N. J.; Doles, J. H., III; and Perkins, F. W.: Deformation and Striation of Plasma Clouds in the Ionosphere. 2. Numerical Simulation of a Nonlinear Two-Dimensional Model. J. Geophys. Res., vol. 78, no. 4, Feb. 1, 1973, pp. 711-724.

7. Haerendel, G.; and Lüst, R.: Electric Fields in the Ionosphere and Magnetosphere. Particles and Fields in the Magnetosphere, B. M. McCormac, ed., Reidel Pub. Co. (Holland), 1971, pp. 213-228.

8. Pilipp, Werner G.: Expansion of an Ion Cloud in the Earth's Magnetic Field, Planet. & Space Sci., vol. 19, no. 9, Sept. 1971, pp. 1095-1119.

9. Adamson, D.; Fricke, C. L.; Long, S. A. T.; Landon, W. F.; and Ridge, D. L.: Preliminary Analysis of NASA Optical Data Obtained in Barium Ion Cloud Experiment of September 21, 1971. J. Geophys. Res., vol. 78, no. 25, Sept. 1, 1973, pp. 5769-5784.

10. Davidson, Robert E.: Ring Structure of a Neutral Gas Cloud Studied in a One-Dimensional Expansion Into Space. NASA TN D-6760, 1972.

11. Staton, Leo D.: The Acceleration of Barium Ion Cloud Striations to Ambient Plasma Velocity. Trans., Amer. Geophys. Union (Abstr. SM7), vol. 53, no. 4, Apr. 1972, p. 483.

12. Mende, S. B.: Morphology of the Magnetospheric Barium Release. J. Geophys. Res., vol. 78, no. 25, Sept. 1, 1973, pp. 5751-5767.

13. Haerendel, G.; Lüst, R.; and Meyer, B.: MPI Analysis of Observations. Barium Releases at Altitudes Between 200 and 1000 Kilometers – A Joint Max-Planck-Institut–NASA Experiment, Hal T. Baber, Jr., Kenneth H. Crumbly, and David Adamson, compilers, NASA SP-264, 1971, pp. 15-27.

14. Haser, L.: Use of Artificial Barium Clouds to Study Magnetic and Electric Fields in the Atmosphere. Aurora and Airglow, Billy M. McCormac, ed., Reinhold Pub. Corp., c.1967, pp. 391-403.

15. Hohl, Frank: Expansion of an Ion Cloud in the Earth's Magnetosphere. J. Geophys. Res., vol. 78, no. 25, Sept. 1, 1973, pp. 5785-5794.

16. Aller, Lawrence H.: Astrophysics – The Atmospheres of the Sun and Stars. Ronald Press Co., c.1953, p. 121.

17. Manring, E. R.; and Patty, R. R.: Yield and Ion Distribution for the Barium Cloud at 31,000 Kilometers, September 21, 1971. J. Geophys. Res., vol. 78, no. 25, Sept. 1, 1973, pp. 5745-5750.

18. Rosenbluth, M. N.; and Longmire, C. L.: Stability of Plasmas Confined by Magnetic Fields. Ann. Phys. (N.Y.), vol. 1, no. 2, May 1957, pp. 120-140.

19. Longmire, Conrad L.: Elementary Plasma Physics. Interscience Publ., 1963, pp. 244-245.